

1 **Enteroendocrine cells switch hormone expression along the crypt-to-villus**
2 **BMP signaling gradient**

3 **Authors:**

4 Joep Beumer¹, Benedetta Artigiani^{1,2}, Yorick Post¹, Frank Reimann³, Fiona Gribble³, Thuc Nghi
5 Nguyen⁴, Hongkui Zeng⁴, Maaïke Van den Born^{1,2}, Johan H. Van Es^{1,2} and Hans Clevers^{1,2*}

7 **Affiliations:**

8
9 ¹ Hubrecht Institute, Royal Netherlands Academy of Arts and Sciences, University Medical
10 Center Utrecht, and University Utrecht, The Netherlands.

11 ² OncoCode Institute, Hubrecht Institute, Utrecht, 3584 CT Utrecht, The Netherlands

12 ³ Metabolic Research Laboratories, Wellcome Trust-MRC Institute of Metabolic Science,
13 Addenbrooke’s Hospital, Cambridge, CB2 0QQ, United Kingdom

14 ⁴ Allen Institute for Brain Science, Seattle, Washington, U.S.A.

15 * Corresponding author: Hans Clevers; h.clevers@hubrecht.eu

29 **Enteroendocrine cells (EECs) control a wide range of physiological processes linked to**
30 **metabolism¹. We show that EECs hormones are differentially expressed between crypts**
31 **(e.g. Glp1) and villi (e.g. Secretin). As demonstrated by single cell mRNA sequencing,**
32 **BMP4 signals can reprogram the expressed repertoire of hormones of individual EECs in**
33 **murine Lgr5⁺ intestinal stem cell-derived organoids. Accordingly, BMP4 induces hormone**
34 **switching of EECs migrating up the crypt-villus axis *in vivo*. This implies the existence of**
35 **fewer EEC lineages in the small intestine than proposed previously. We also describe a**
36 **protocol to generate human EECs in organoids and demonstrate that BMP signaling**
37 **regulates hormone expression in a similar fashion. These observations suggest strategies to**
38 **pharmacologically manipulate numbers of EECs expressing therapeutically relevant**
39 **hormones, such as Glp1.**

40 The EECs of the intestine together constitute the largest hormone-producing organ in mammals.
41 EECs are classified according to their hormone products¹. Enterochromaffin cells (ECs) produce
42 Serotonin, a regulator of intestinal motility, and Tachykinin 1 (Tac1), also known as Substance
43 P, a peptide which is believed to play a role in muscle contraction and inflammation². L-cells
44 produce Glp1, an inducer of insulin release encoded by the Glucagon (Gcg) gene, and can co-
45 express Pyy¹. Other EEC subtypes include Gastric inhibitory protein (Gip)-producing K-cells,
46 Somatostatin (Sst)-producing D-cells, Cholecystokinin (Cck)-producing I-cells, Neurotensin
47 (Nts)-producing N-cells and Secretin (Sct)-producing S-cells¹. Although this classification
48 suggests well-defined, distinct subtypes of EECs, these hormones are often co-expressed
49 suggesting considerable overlap between lineages^{3,4}. Like all other cell types of the intestinal
50 epithelium, the short-lived EECs are constitutively produced by Lgr5⁺ crypt stem cells⁵. Lgr5

51 stem cells can be cultured to generate epithelial organoids that faithfully recapitulate gut
52 epithelial biology⁶. Single cell sequencing has shown that a complete set of EECs subtypes is
53 produced in these mini-guts, including some that had previously gone unnoticed in intact gut^{7,8}.
54 However, extrinsic factors that control EEC subtype identity have remained largely unknown.

55 Previous work has suggested that EECs expressing Tac1 and Glp1 are restricted to crypts, while
56 Sct-, Pyy- and Nts-producing EECs are enriched in villi^{9,10}. In agreement with these studies, we
57 found that ileal L-cells co-express Glp1 and Pyy in the crypt, but mostly lack Glp1 in the villus
58 (Fig. 1a-c, Fig. S1a). Serotonin-producing ECs occur along the length of the crypt-villus axis, but
59 selectively co-express Tac1 in the crypt and Sct in the villus (Fig. 1d-e, Fig. S1a). To address if
60 hormone switching occurs during migration of EECs along the crypt-villus axis, we analyzed
61 intestines from *Tac1^{iresCre} / Rosa^{tdTomato}* mice, an allele which faithfully labels all Tac1⁺/Serotonin⁺
62 cells in the crypt (Fig. 1f)¹¹. In adult intestines, almost all Serotonin⁺ cells were marked by
63 tdTomato (Fig. 1g). Importantly, >55% of Sct⁺ cells on villi were also traced, while being
64 negative for Tac1 (Fig. 1f-g, S1b). The rarity of tdTomato⁺ cells that were negative for Serotonin
65 suggests that ECs do not lose Serotonin during their lifetime to become single Sct⁺ as previously
66 suggested^{9,12}. Sct⁺ cells that are not traced by Tac1 and are Serotonin-negative must thus be part
67 of another EEC lineage. EECs producing other hormones, including Cck, Gip and Sst, were only
68 very rarely derived from Tac1⁺ progenitors (Fig. 1g, S1b). These tracing data implied lineage
69 relationships between crypt and villus EECs, i.e that Tac1⁺/Sct⁺ ECs on villi derive from Tac1⁺
70 crypt ECs. This in turn suggested that local niche signals could induce shifts in hormone
71 expression.

72

73 Multiple signaling gradients exist along the crypt-villus axis, e.g. Wnt levels are high at the crypt
74 base, while BMP is highest at the villus tips^{13,14}. Induction of EECs in murine intestinal
75 organoids can be achieved through inhibition of the Wnt, MAPK and Notch signaling pathways,
76 in the presence of the BMP inhibitor Noggin⁸. We used this differentiation system as a starting
77 point to modulate selected signaling pathways⁸, while monitoring Sct and Gcg as a proxy of the
78 villus- and crypt-hormone signatures respectively. Strikingly, we observed that all ECs in this
79 culture co-expressed Serotonin and Tac1, while Sct was absent (Fig. 2a). This suggests niche
80 signals acting on EECs are dominant over a default, temporal differentiation process.
81 Manipulation of the Wnt, TGF β and Hedgehog pathways did either reduce both Gcg and Sct
82 transcripts, or had no significant on any assessed hormone (Fig. S2a). We then replaced Noggin
83 by BMP4 in this EEC differentiation cocktail ('EEC BMP^{high}' medium), generating cells
84 immunoreactive for Sct, as well as ECs lacking Tac1 (Fig. 2a-b). Glp1⁺ cell numbers and total
85 levels of secreted Glp1 were greatly diminished (Fig. 2a-c, S2b). We next performed bulk RNA
86 sequencing on duodenal and ileal organoids stimulated with EEC BMP^{high} or EEC BMP^{low} media
87 (Fig. 2d), and validated the expression of selected genes by qPCR (Fig. 2e). EEC markers which
88 are homogenously distributed on crypts and villi (Chga, Tph1 (enzyme catalyzing Serotonin
89 production), Cck and duodenal Gip) are only mildly affected by BMP activation (Fig. 2d-e). We
90 did observe an increase in Sct and a minor upregulation of Pyy and Nts (Fig. 2d-e), which are
91 expressed highest in the villus¹⁰. Sct is reported to be enriched in the proximal part of the SI¹, but
92 we observe that our EEC differentiation protocol generates Sct⁺ cells equally well in the proximal
93 and distal SI organoids. Trpa1, an irritant receptor enriched in EECs of the intestinal crypt¹⁵,
94 decreased with BMP activation (Fig. 2d). BMP4-mediated changes in hormone expression could

95 be overridden by the addition of BMPR1a inhibitor LDN193189, confirming involvement of the
96 BMPR1/2 axis (Fig. S2c-d).

97 To address whether BMP signaling can switch hormone expression in individual mature EECs
98 rather than selectively depleting subtypes of EECs, we followed the fate of Gcg- or Tac1-
99 expressing cells using cultures derived from *Gcg^{Venus}* and *Tac1^{iresCre} /Rosa26^{tdTomato}* mice^{11,16}.
100 Live-cell imaging of *Gcg^{Venus}* organoids demonstrated that BMP activation induced a decrease in
101 Venus levels, suggesting downregulation of Gcg (Fig. S2e-f). We did not observe BMP-induced
102 apoptosis of Venus⁺ or tdTomato⁺ cells (Fig. S2g).

103 Changes in hormone expression in individual EECs might be caused by dynamics in
104 transcriptional networks, and accompanied by production of other sensory receptors. To identify
105 dynamics at a single cell level, we performed single cell RNA sequencing of traced Tac1-, Glp1-
106 or Gip-expressing murine cells¹⁶. Gip⁺ K-cells exist both in crypts and villi and were isolated
107 from organoids derived from a *Gip^{Cre} /Rosa26^{tdRFP}* mouse¹⁷. Guided by their regional *in vivo*
108 abundance, we isolated organoids from the proximal SI of the Gip-, from the distal SI of Gcg-
109 and from the whole SI of Tac1 reporter mice. Organoids were treated with a MEK inhibitor to
110 limit new EEC generation and either exposed to Noggin (control) or BMP4 for 24 or 96 hours
111 (Fig. 3a). Next, EECs derived from the reporters/treatments were sorted for the reporter
112 fluorescence and single cell RNA sequencing was performed using SORTseq¹⁸, an automated
113 version of CELseq2 (Fig. 3a, S3a)¹⁹. K-medoids clustering by RaceID2 algorithm²⁰ showed that
114 Tac1-, Gcg- and Gip-traced cells, classically defined as ECs, L- and K- cells respectively,
115 clustered accordingly to their cell-type and mostly independently of the treatment in a t-SNE
116 space (Fig. 3b-c). We identified Alpi⁺ enterocytes and Muc2⁺ Goblet cells derived from the

117 *Gcg*^{Venus} reporter that displayed the lowest Venus fluorescence intensity (Fig. S3b). We also
118 detected a cluster of unknown identity with expression of the vomeronasal receptor *Vmn2r55*,
119 which was identified previously⁷. BMP-stimulated ECs displayed lower *Sct* expression
120 compared to L- and K-cells (Fig. 3c-e). Within ECs, expression of *Tph1* remained unchanged
121 during BMP treatment, while *Tac1* decreased (Fig. 3c-e). Cells clustering as classical L-cells
122 dramatically reduced their *Gcg* (*Glp1*) expression, while activating *Nts* and *Pyy* transcription
123 following BMP treatment (Fig. 3d and S3c). Some *Gcg*^{Venus}-sorted cells from ileal organoids
124 expressed *Gip*, combined with low levels of *Gcg* (Fig. 3b-d). These cells clustered together with
125 K-cells and could not be induced to express *Nts*, indicating that these cells represent K-cells and
126 not L-cells. (Fig. 3d). L-cells and to a lesser extent K-cells express *Cck* independent of treatment
127 (Fig. 3d). Within *Gip*-traced K-cells, we observed a separate population of *Sst*-producing cells.
128 BMP activation had no effect on *Sst* expression and caused a mild reduction in *Gip* expression in
129 these clusters, while activating *Sct* expression only in *Gip*⁺ but not in *Sst*⁺ cells (Fig. 3d-e, S3c).
130 *Pyy* expression could be induced in both *Gip*⁺ and in *Sst*⁺ cells, but to a lesser extent than in L-
131 cells (Fig. S3c). We did observe low *Cck*, *Gcg* and no *Nts* expression in K-cells, indicating that
132 these represent a separate lineage from ileal L-cells (Fig. 3d-e).

133 We identified uniquely expressed genes in the various clusters, that corresponded to
134 known expression or function along the crypt-to-villus axis *in vivo*. The irritant receptor *Trpa1*
135 (proposed to be involved in serotonin release) has been shown to be enriched in the crypt^{15,21}.
136 Concordantly, it decreases during BMP treatment within ECs (Fig. 3d-e). We find the orphan
137 receptor *Asic5* to be expressed by *Sst*⁺ cells (Fig. S3d). This same population also expresses the
138 islet amyloid polypeptide (*Iapp*) Amylin (Fig. S3d), a peptide previously found in pancreatic β -

139 cells and known to have a wide range of metabolic effects²². The LIM homeobox factor *Lmx1a*
140 occurs in ECs, as suggested recently²³. The homeobox protein *Hhex* -not previously observed in
141 the gut- was expressed by *Sst*-producing cells (Fig. S3d). Interestingly, it has been described as
142 an essential factor for *Sst*-producing δ cells in the pancreas²⁴. The T-box transcription factor
143 *Tbx3* is produced in BMP-activated EECs (Fig. S3d), and is enriched in the villus²⁵. Finally, we
144 find specific activation of classical BMP target genes in BMP-treated cells, such as *Id1*, *Id2* and
145 *Id3*, confirming pathway activation (Fig. S3d)²⁶.

146 Transcript dynamics might not be fully predictive for changes at the peptide hormone
147 level. Therefore, we repeated the same experimental strategy as for the single cell RNA
148 sequencing and assessed co-expression of relevant peptide hormones in the *Tac1^{iresCre}*
149 */Rosa26^{tdTomato}*- and *Gcg^{Venus}*- reporter organoids. Over the course of 4 days, BMP-inhibited
150 *tdTomato*⁺ cells remained immunoreactive for *Tac1* and Serotonin, while only rarely expressing
151 *Sct* (Fig S4a). Strikingly, BMP-activated *tdTomato*⁺ cells lost *Tac1* immunoreactivity,
152 maintained Serotonin and gained *Sct* positivity (Fig S4a). *Glp1* positivity was strongly correlated
153 with Venus expression in *Gcg^{Venus}* organoids in BMP-untreated conditions, while this correlation
154 is lost in BMP-treated samples (Fig. S4a). Conversely, Venus positivity was increasingly
155 predictive for *Sct* expression after BMP treatment (Fig. S4a). *Pyy* peptide positivity remained
156 unchanged irrespective of BMP treatment (Fig S4a), in line with the constant peptide levels
157 between crypt and villus *in vivo*¹⁰.

158 We performed live cell imaging of the *Tac1^{iresCre}* */Rosa26^{tdTomato}*- and *Gcg^{Venus}*- reporter
159 organoids in BMP-untreated and -treated conditions. *tdTomato*⁺ cells that existed at the
160 beginning of the BMP treatment continued to persist over the course of 60 hours, while losing

161 Tac1 and gaining Sct expression (Fig. S4b). Untreated cells retained Tac1 positivity (Fig. S4b).
162 In Gcg^{Venus} - reporter organoids, we observed a similar increase in Sct peptides (Fig. S4b).
163 Collectively, these data indicated that individual EECs can rewire their peptide hormone profile
164 upon activation of BMP signaling.

165 The number of tdTomato⁺ and Venus⁺ EECs increased significantly more over 4 days when BMP
166 signaling is inhibited compared to when activated (Fig. S4a). We found that the first transcription
167 factor expressed by and defining the EEC lineage, Neurogenin 3²⁷, is inhibited by BMP
168 activation (Fig. S4c). To circumvent a bias that occurs at the bulk population level due to this
169 inhibition of EEC specification, we first generated a large pool of ileal EECs using our
170 differentiation protocol for 3 days. Next, we switched to BMP-high conditions for 24 hours (Fig.
171 S4d). Increases in Sct, Pyy and Nts expression were more pronounced compared to a continuous
172 BMP inhibition (Fig. 2 and Fig. S4c). These data imply that initial EEC specification requires
173 BMP low conditions, such as exists at the bottom of the crypt.

174 To investigate whether villus-produced BMP controls hormone expression *in vivo*, we
175 analyzed intestines from mice that ectopically express BMP inhibitor Noggin in the intestinal
176 epithelium (Villin^{Noggin})¹³. As expected, we observed an increased expression of Tac1 and Glp1
177 in the villi of these mice, while Sct was reduced (Fig S5a-d). We next tested the feasibility of
178 influencing hormone expression by targeting the BMP gradient with the BMPR1a inhibitor
179 LDN193189²⁸. An 80-hour oral treatment caused a reduction in Sct⁺ cell numbers. Overall
180 histology of the intestine was unaffected, and the number of Chga⁺ EECs did not change
181 significantly (Fig. 4a-b), consistent with a previous study showing no change in Chga after BMP
182 inhibition²⁹. We quantified the numbers of Tac1⁺ and Glp1⁺ along different segments of the

183 crypt-villus axis, assuming that BMP inhibition would not increase these in the BMP-low crypt.
184 BMP inhibition did not cause significant changes in the lowest crypt-villus segment in the
185 number of Tac1⁺ or Glp1⁺ EECs (Fig. 4a, 4c). However, the increase in cells immunoreactive for
186 Tac1 or Glp1 was very pronounced higher up in the villus (Fig. 4a, 4c).

187 Finally, we pursued the establishment of a differentiation platform for induction of EECs
188 in human intestinal organoids³⁰. Best results were obtained with dual inhibition of Notch and
189 MEK signaling (Fig. 5a-b). This allowed us to generate all subtypes of EECs in organoids either
190 derived from human duodenal or ileal tissue. ENR differentiated organoids did not contain EECs
191 but mostly enterocytes, as evidenced by their extensive brush border (Fig. 5a). In our EEC
192 differentiation protocol, BMP activation induced similar trended alterations in EEC hormone
193 repertoires as it did in murine organoids (Fig. 5c). *NTS* and *SCT* transcripts increased upon BMP
194 stimulation, while we observed a dramatic reduction in *GCG* (Fig. 5c). BMP activation had a
195 neutral effect on total *CHGA* expression, and in contrast to the mouse, *PYY* was not increased
196 upon BMP stimulation (Fig. 5c). Although cells positive for both GLP1 and NTS peptides were
197 observed in control conditions, we only observed NTS single positive cells in BMP-treated
198 conditions (Fig. 5d). This implies that BMP-control of the expressed EEC hormone repertoire is
199 a generalizable phenomenon. In line with our observations in the murine organoid system⁸, we
200 find that human intestinal organoids maintain their regional identity in terms of representation of
201 EEC subtypes. *GCG*, *NTS* and *PYY* were highly enriched in distal gut organoids, while *CCK*
202 displays a much higher bias towards the duodenum (Fig. 5c).

203 Taken together, these data provide two main insights into EEC biology. First, the
204 observations support that BMP controls hormone expression of EECs. EECs that are born in

205 crypts from *Lgr5* stem cells encounter increasing levels of BMP signaling when migrating
206 towards the villus tips³¹, and can change their hormone profile during this journey. Second, this
207 insight in combination with the single cell sequencing data proposes a simplification of EEC
208 taxonomy (Fig. 5e). Confusingly, previous high resolution imaging and single cell RNA
209 sequencing has suggested that almost every combination of EEC hormones can occur in
210 individual EECs³². Our current data indicate that there might be fewer unrelated differentiation
211 pathways of EECs ('lineages') than previously anticipated and that some of the marker-hormones
212 indeed are not hard-wired. Our data imply that there might exist no EECs uniquely dedicated to
213 the production of Sct or Nts (the so called S- or N-cells) or Pyy, and that most EECs initiate
214 expression of Sct when entering the BMP-high villus domain. Indeed, we observe that all BMP-
215 activated EECs except D-cells upregulate Sct to different degrees, while L-cells (but not Sst- or
216 Serotonin-producing cells) increase Pyy and Nts. Gip-expressing cells can be induced to express
217 lower levels of Pyy, but not Nts. Importantly, we find that Chga is a marker of Serotonin-positive
218 cells but not of other EECs, and using it as a generic marker would not allow for identifying EEC
219 regulators such as the BMP pathway.

220 Pulse-chase labeling using BrdU has indicated that EECs do not necessarily follow the conveyor-
221 belt migration pattern in which cells follow a constant flow from the bottom of the crypt to the
222 tip of the villus^{12,33}. Recently it has been shown that EECs can physically interact with enteric
223 neurons through synapses, which potentially could alter cellular migration^{34,35}. Subpopulations
224 of EECs can be retained in the crypt for 2 weeks while maintaining expression of Tac1 or Glp1.
225 Cells that migrate onto the villus are destined to lose Tac1 or Glp1^{9,12,33}. This ultimately suggests

226 that controlling EEC migration along the crypt-villus axis and the Wnt and BMP gradients would
227 be a way to influence hormone expression patterns.

228

229 **Figure legends**

230 **Fig. 1 Enteroendocrine cells switch hormone expression while migrating from crypt to**
231 **villus. a and b**, Immunohistochemical analysis reveals Glp1⁺ cells are enriched in the ileal crypt,
232 where they co-express Pyy. Experiment in (a) was repeated two times independently with similar
233 results. c, Quantification of b. The percentage of Pyy⁺ cells that co-express Glp1 are represented
234 in the lower chart. d, ECs express Tac1 in the crypt and Sct in the villus, while Serotonin is
235 produced in both locations. e, Quantification of d. The percentage of Serotonin⁺ cells that co-
236 express Tac1 or Sct are represented in the lower charts. f, Intestine of Tac1^{iresCre} /Rosa^{Ai14} mice
237 reveals that ECs lose Tac1 and gain Sct expression from crypt to villus. g, Quantification of (f)
238 and Fig S1. The percentages of each hormone that is tdTomato⁺ (upper chart) and of tdTomato⁺
239 cells that are hormone positive (lower chart) are shown. The mean values are depicted in graphs
240 c, e and g, and error bars present SD for n=4 mice for each experiment. Scale bar is 50 μ m.

241 **Fig.2 Activation of BMP signaling induces Villus-like hormone signature in mouse EECs.**

242 **a**, Organoids are differentiated for 4 days to EECs in the absence (EEC BMP_{low}) or presence of
243 BMP4 (EEC BMP_{high}). ENR is used as a control. Activation of BMP signaling induces
244 expression of Sct, while repressing Tac1 and Glp1. Images are presented as maximum
245 projections. **b**, Quantification of a. The number of positive cells for each hormone were
246 quantified and are displayed per mm of organoid epithelium. The percentage of Serotonin⁺ cells
247 that co-express Tac1 are presented. Sample size represents n=2 biologically independent
248 experiments, in which at least 3 organoids were quantified per replicate and staining. Statistics
249 were derived comparing all organoids (n=12 for Sct, n=6 for other hormones) in BMP low and
250 high conditions using a two-sided t-test. Mean values per treatment are shown, and error bars

251 present SD. **c**, Overlay of brightfield and Venus image of organoids derived from Gcg^{Venus} mice
252 after a 4 day treatment with a BMP_{low} or BMP_{high} EEC differentiation cocktail. BMP
253 activation represses expression of Gcg , without inducing morphological alterations. Experiment
254 was repeated independently 10 times. **d**, Volcano plots showing results from RNA sequencing of
255 organoids stimulated for 4 days with BMP low or high EEC differentiation cocktails, from
256 proximal (left) and distal (right) SI organoids. Gene expression fold change (\log_2) of BMP^{high}
257 versus BMP^{low} is shown on the x -axis and significance on the y -axis. Each grey dot represents a
258 gene, and dots representing relevant genes are highlighted in different colors, according to their
259 function. Sample size represents $n=2$ biologically independent experiments, and p -adjusted
260 values were calculated with a Wald test using the DESeq2 package. **e**, qPCR analysis of
261 selected hormones from **d**. Expression levels are shown relative to control organoids in ENR
262 medium. Experiment was performed in $n=2$ biologically independent experiments, and the mean
263 expression is depicted. Scale bar is 50 μm .

264 **Fig.3 Single cell RNA sequencing reveals BMP regulated plasticity among different EEC**
265 **subtypes. a**, Experimental paradigm. Different EEC reporter organoids were treated with a MEK
266 inhibitor, while receiving Noggin or BMP4. After 4 days, organoids were dissociated and traced
267 EECs sorted and processed for single cell RNA sequencing. **b** and **c**, t-SNE map of single cell
268 RNA sequenced EECs using the RaceID2 algorithm. Different colors, as indicated in the legend,
269 highlight cells isolated from different reporter organoids (**b**) and treatments (**c**). **d**, Expression
270 levels of selected hormones and receptors in the tSNE space of (**b-c**). **e**, Expression of individual
271 hormones within different EEC reporter sorted cells are presented in violin plots, with different
272 colors for the different treatments (as indicated in the legend). Violin plots depict median values

273 (white dot), 50% of the values (within thick black line) and 95% of the values (within thin black
274 line). The number of cells per treatment and reporter is depicted. Different dynamics of hormone
275 expression were observed over the course of BMP treatment in subtypes of EECs.

276 **Fig. 4 Manipulation of BMP gradient alters hormone expression in mice.** **a**, Mice were
277 treated for 80 hours with BMP α inhibitor LDN193819. Immunohistochemical analysis of the
278 intestine shows a repression of Sct and induction of Glp1 and Tac1 expression upon BMP
279 inhibition. Glp1⁺ and Tac1⁺ expressing cells are mostly restricted to the crypt in control mice, but
280 expand into the upper villus region upon BMP inhibition. **b**, Quantification of **a**. Number of
281 Chga⁺ and Sct⁺ positive cells per treatment. **c**, Quantification of **a**. Number of Tac1⁺ or Glp1⁺
282 cells are displayed for each segment of the crypt-villus axis in the different treatments. Cells
283 positive for Tac1 and Glp1 increase in the higher villus segments upon LDN193819 treatment.
284 Tac1⁺ cells are counted and displayed in 10mm of the proximal small intestine. Glp1⁺ cells are
285 counted and displayed in 30mm of the distal small intestine. Results presented are derived from
286 n=4 mice per treatment, and statistics were calculated using a two-sided t-test. Mean values per
287 staining and treatment are shown, and error bars present SD. Scale bar is 50 μ m.

288 **Fig. 5 New human EEC differentiation protocol implies conserved BMP-controlled**
289 **hormone expression.** **a**, Human small intestinal organoids were induced to differentiate either
290 for 5 days by withdrawing Wnt signals (ENR) or to EECs through additional MEK and Notch
291 inhibition. Immunofluorescence indicates the presence of different subtypes of EECs in human
292 organoids. White arrows indicate NTS⁺ cells, red arrows GLP1⁺ cells. Experiment has been
293 repeated four times independently with similar results. **b**, Brightfield images of human intestinal
294 organoids in expansion medium or after a 5 day differentiation towards EECs. Experiment was

295 repeated independently four times. **c**, The 5-day differentiation protocol of EECs ('humanEEC')
296 was performed in the presence and absence of BMP4. Expression levels of hormones were
297 determined by qPCR and are shown relative to duodenal ENR control. Gcg expression is shown
298 relative to ileal ENR control, as it was not detected in duodenal organoids. Sample size
299 represents n=2 biologically independent experiments, and the mean expression values are shown.
300 **d**, Human EECs were produced in the absence (BMP_{low}) or presence (BMP_{high}) of BMP4.
301 NTS overlaps with GLP1 in BMP low conditions, while only NTS single positive cells are
302 observed in BMP_{high} conditions. Experiment was repeated independently four times. Scale bar
303 is 50 μ m. **e**, Model of EEC differentiation. K-cells are enriched in the proximal and L-cells in the
304 distal part of the SI respectively, whereas ECs and D-cells are uniformly distributed. A crypt-to-
305 villus BMP signaling gradient drives alterations in hormone repertoires in these EEC lineages.

306

307

308

309

310

311

312

313

314

315

316

317

318 **Acknowledgements**

319 We thank Stefan van der Elst, Reinier van der Linden and Yotam Bar-Ephraim, for their help
320 with FACS experiments. B.A. is supported by NWO/VENI 863.15.015.

321 **Competing financial interests**

322 The authors disclose no conflicts of interest.

323 **Author contributions**

324 J.B. and H.C. conceived and designed the project. J.B. designed and performed all experiments.
325 B.A. performed analysis of RNA sequencing data. F.R. and F.G. generated the Gcg and Gip
326 reporter mice. H.Z. generated the Tac1 reporter mouse, and T.N.N. assisted in providing the
327 tissue. J.H.v.E supervised and performed the mouse experiments, with the help of M.v.d.B. Y.P.
328 assisted in histology preparation. J.B., B.A. and H.C. wrote the manuscript with input from all
329 other authors.

330

331

332

333

334

335

336

337 **References**

- 338 1. Furness, J. B., Rivera, L. R., Cho, H.-J., Bravo, D. M. & Callaghan, B. The gut as a
339 sensory organ. *Nat. Rev. Gastroenterol. Hepatol.* **1010**, 729–740 (2013).
- 340 2. Connor, T. M. O. *et al.* The Role of Substance P in Inflammatory Disease.
341 doi:10.1002/jcp.20061
- 342 3. Egerod, K. L. *et al.* A major lineage of enteroendocrine cells coexpress CCK, secretin,
343 GIP, GLP-1, PYY, and neurotensin but not somatostatin. *Endocrinology* **153**, 5782–5795
344 (2012).
- 345 4. Haber, A. L. *et al.* A single-cell survey of the small intestinal epithelium. *Nature* **551**,
346 333–339 (2017).
- 347 5. Barker, N. *et al.* Identification of stem cells in small intestine and colon by marker gene
348 *Lgr5*. *Nature* **449**, 1003–1007 (2007).
- 349 6. Sato, T. *et al.* Single *Lgr5* stem cells build crypt-villus structures in vitro without a
350 mesenchymal niche. *Nature* **459**, 262–265 (2009).
- 351 7. Grün, D. *et al.* Single-cell messenger RNA sequencing reveals rare intestinal cell types.
352 *Nature* **525**, 251–5 (2015).
- 353 8. Basak, O. *et al.* Induced Quiescence of *Lgr5*+ Stem Cells in Intestinal Organoids Enables
354 Differentiation of Hormone-Producing Enteroendocrine Cells. *Cell Stem Cell* **20**, 177–
355 190.e4 (2017).
- 356 9. Roth, K. a & Gordon, J. I. Spatial differentiation of the intestinal epithelium: analysis of
357 enteroendocrine cells containing immunoreactive serotonin, secretin, and substance P in
358 normal and transgenic mice. *Proc. Natl. Acad. Sci. U. S. A.* **87**, 6408–6412 (1990).
- 359 10. Grunddal, K. V. *et al.* Neurotensin is coexpressed, coreleased, and acts together with
360 GLP-1 and PYY in enteroendocrine control of metabolism. *Endocrinology* **157**, 176–194
361 (2016).
- 362 11. Harris, J. A. *et al.* Anatomical characterization of Cre driver mice for neural circuit
363 mapping and manipulation. *Front. Neural Circuits* **8**, (2014).
- 364 12. Aiken, K. D. & Roth, K. A. Temporal differentiation and migration of substance P,
365 serotonin, and secretin immunoreactive enteroendocrine cells in the mouse proximal small
366 intestine. *Dev. Dyn.* **194**, 303–310 (1992).
- 367 13. Haramis, A.-P. G. De novo crypt formation and Juvenile Polyposis on BMP inhibition in
368 mouse intestine. *Science (80-.).* **303**, 1684–1686 (2004).
- 369 14. Beumer, J. & Clevers, H. Regulation and plasticity of intestinal stem cells during
370 homeostasis and regeneration. *Development* **143**, 3639–3649 (2016).

- 371 15. Camacho, S. *et al.* Anti-obesity and anti-hyperglycemic effects of cinnamaldehyde via
372 altered ghrelin secretion and functional impact on food intake and gastric emptying. *Sci.*
373 *Rep.* **5**, 7919 (2015).
- 374 16. Habib, A. M. *et al.* Overlap of endocrine hormone expression in the mouse intestine
375 revealed by transcriptional profiling and flow cytometry. *Endocrinology* **153**, 3054–3065
376 (2012).
- 377 17. Svendsen, B. *et al.* GLP1- and GIP-producing cells rarely overlap and differ by bombesin
378 receptor-2 expression and responsiveness. *J. Endocrinol.* **228**, 39–48 (2016).
- 379 18. Muraro, M. J. *et al.* A Single-Cell Transcriptome Atlas of the Human Pancreas. *Cell Syst.*
380 **3**, 385–394 (2016).
- 381 19. Hashimshony, T. *et al.* CEL-Seq2: sensitive highly-multiplexed single-cell RNA-Seq.
382 *Genome Biol.* **17**, 77 (2016).
- 383 20. Grün, D. *et al.* De Novo Prediction of Stem Cell Identity using Single-Cell Transcriptome
384 Data. *Cell Stem Cell* **19**, 266–277 (2016).
- 385 21. Nozawa, K. *et al.* TRPA1 regulates gastrointestinal motility through serotonin release
386 from enterochromaffin cells. *Proc. Natl. Acad. Sci. U. S. A.* **106**, 13 (2009).
- 387 22. X.-X., Z., Y.-H., P. & Y.-M., H. Neuroendocrine hormone amylin in diabetes. *World J.*
388 *Diabetes* **7**, 189–197 (2016).
- 389 23. Gross, S. *et al.* The novel enterochromaffin marker *Lmx1a* regulates serotonin
390 biosynthesis in enteroendocrine cell lineages downstream of *Nkx2.2*. *Development* **143**,
391 2616–2628 (2016).
- 392 24. Zhang, J., McKenna, L. B., Bogue, C. W. & Kaestner, K. H. The diabetes gene *Hhex*
393 maintains α -cell differentiation and islet function. *Genes Dev.* **28**, 829–834 (2014).
- 394 25. Kaaij, L. T. *et al.* DNA methylation dynamics during intestinal stem cell differentiation
395 reveals enhancers driving gene expression in the villus. *Genome Biol.* **14**, R50 (2013).
- 396 26. Hollnagel, A., Oehlmann, V., Heymer, J., Rüther, U. & Nordheim, A. *Id* genes are direct
397 targets of bone morphogenetic protein induction in embryonic stem cells. *J. Biol. Chem.*
398 **274**, 19838–19845 (1999).
- 399 27. Jenny, M. *et al.* Neurogenin3 is differentially required for endocrine cell fate specification
400 in the intestinal and gastric epithelium. *EMBO J.* **21**, 6338–6347 (2002).
- 401 28. Whissell, G. *et al.* The transcription factor GATA6 enables self-renewal of colon adenoma
402 stem cells by repressing BMP gene expression. *Nat. Cell Biol.* **16**, 695–707 (2014).
- 403 29. Qi, Z. *et al.* BMP restricts stemness of intestinal *Lgr5*⁺ stem cells by directly suppressing
404 their signature genes. *Nat. Commun.* **8**, 13824 (2017).
- 405 30. Sato, T. *et al.* Long-term expansion of epithelial organoids from human colon, adenoma,

- 406 adenocarcinoma, and Barrett's epithelium. *Gastroenterology* **141**, 1762–1772 (2011).
- 407 31. Clevers, H. The intestinal crypt, a prototype stem cell compartment. *Cell* **154**, 274–284
408 (2013).
- 409 32. Fothergill, L. J., Callaghan, B., Hunne, B., Bravo, D. M. & Furness, J. B. Costorage of
410 enteroendocrine hormones evaluated at the cell and subcellular levels in male mice.
411 *Endocrinology* **158**, 2113–2123 (2017).
- 412 33. Aiken, K. D., Kisslinger, J. A. & Roth, K. A. Immunohistochemical studies indicate
413 multiple enteroendocrine cell differentiation pathways in the mouse proximal small
414 intestine. *Dev. Dyn.* **201**, 63–70 (1994).
- 415 34. Bellono, N. W. *et al.* Enterochromaffin Cells Are Gut Chemosensors that Couple to
416 Sensory Neural Pathways. *Cell* **170**, 185–198.e16 (2017).
- 417 35. Bohorquez, D. V *et al.* Neuroepithelial circuit formed by innervation of sensory
418 enteroendocrine cells. *J Clin Invest* **125**, 782–786 (2015).
- 419 36. Farin, H. F. *et al.* Visualization of a short-range Wnt gradient in the intestinal stem-cell
420 niche. *Nature* **530**, 340–343 (2016).
- 421 37. Muñoz, J. *et al.* The Lgr5 intestinal stem cell signature: robust expression of proposed
422 quiescent '+4' cell markers. *EMBO J.* **31**, 3079–3091 (2012).
- 423 38. Li, H. & Durbin, R. Fast and accurate short read alignment with Burrows-Wheeler
424 transform. *Bioinformatics* **25**, 1754–1760 (2009).
- 425 39. Love, M. I., Huber, W. & Anders, S. Moderated estimation of fold change and dispersion
426 for RNA-seq data with DESeq2. *Genome Biol.* **15**, 550 (2014).
- 427 40. Grün, D., Kester, L. & van Oudenaarden, A. Validation of noise models for single-cell
428 transcriptomics. *Nat. Methods* **11**, 637–640 (2014).
- 429

1 **Methods**

2 **Mouse strains and experiments**

3 Primary organoid cultures used in this culture were derived from Gcg^{Venus} , $Tac1^{iresCre}$
4 $/Rosa26^{tdTomato}$ and $Gip^{iresCre}/Rosa26^{tdRfp}$ mice^{11,16}, and established as described before⁶. All mice
5 were bred on a C57BL/6 background. All animal procedures and experiments were performed in
6 accordance with national animal welfare laws under a project license obtained from the Dutch
7 Government, and were reviewed by the Animal Ethics Committee of the Royal Netherlands
8 Academy of Arts and Sciences (KNAW). All rodents are housed in a barrier facility in
9 conventional cages and are changed without using a change stations. All personnel entering the
10 barrier must wear protective clothing (including head caps, special clogs). All animals are
11 received directly from approved vendors (Charles River) or generated in house. Animals arriving
12 from other sources must pass the GDL –quarantine for screening or by embryo-transfer. After
13 screening these SPF mice are housed in micro isolator cages and are transferred to the Hubrecht
14 laboratory.

15 For the BMPR inhibition experiment, LDN193189 (Selleckchem) was dissolved in citric buffer
16 (pH3-3.1) at 2mg ml^{-1} . 12 week old mice ($n=4$) were given two oral doses of LDN193189 at 17.5
17 mg per kg bodyweight per day. Citric buffer was given to control mice. The total treatment was
18 maintained for 80 hours. All mouse experiments were conducted under a project license granted
19 by the Central Committee Animal Experimentation (CCD) of the Dutch government and
20 approved by the Hubrecht Institute Animal Welfare Body (IvD), with project license number
21 AVD8010020151.

22

23

24 **Murine and human intestinal organoid culture**

25 The basic culture medium (advanced Dulbecco's modified Eagle's medium/F12 supplemented
26 with penicillin/streptomycin, 10 mM HEPES, Glutamax, B27 [Life Technologies, Carlsbad, CA]
27 and 1 mM N-acetylcysteine [Sigma]) was supplemented with 50 ng/ml murine recombinant
28 epidermal growth factor (EGF; Peprotech, Hamburg, Germany), R-spondin1 (conditioned
29 medium, 5% final volume), and Noggin (conditioned medium, 5% final volume), called "ENR"
30 medium. Conditioned media were produced using HEK293T cells stably transfected with HA-
31 mouse Rspo1-Fc (gift from Calvin Kuo, Stanford University) or after transient transfection with
32 mouse Noggin-Fc expression vector. Advanced Dulbecco's modified Eagle's medium/F12
33 supplemented with penicillin/streptomycin, and Glutamax was conditioned for 1 week.

34 Human duodenal and ileal tissues were obtained from the UMC Utrecht with informed consent
35 of each patient. The study was approved by the UMC Utrecht (Utrecht, The Netherlands) ethical
36 committee and was in accordance with the Declaration of Helsinki and according to Dutch law.
37 Patients were diagnosed with a small or large intestinal cancer and from the resected intestinal
38 segments, a sample was taken from normal mucosa for this study. Human small intestinal cells
39 were isolated, processed and cultured as described previously³⁰.

40 Organoids were plated in BME (Trevigen). MEK signaling was inhibited using PD0325901
41 (1 μ M for murine, 100nM for human organoids; Sigma Aldrich). Wnt secretion was inhibited
42 with IWP-2 (5 μ M; Stemgent) and Notch with DAPT (10uM, Sigma Aldrich). BMP signaling
43 was activated by treating with human recombinant BMP4 (20ng/ml, Peprotech) and withdrawal
44 of Noggin from the culture medium. Hedgehog signaling was inhibited with Vismodegib (10uM,
45 Selleckchem). TGF beta signaling was activated using recombinant mouse TGF beta-1 (3ng ml⁻¹,
46 R&DSsystems, MAB7666TGF beta-1. TGF beta type1 receptor signaling was inhibited using

47 A83 (500nM, Tocris). All control organoids were treated with similar concentrations of the
48 compound solvent, dimethyl sulfoxide (DMSO) or 0.1%BSA in PBS0. During treatments,
49 cells were imaged using an EVOS microscope (Electron Microscopy Sciences).

50 For the induction of enteroendocrine differentiation in murine organoids, cells were cultured in
51 standard culture conditions (ENR). 4-7 days after plating in BME, medium was removed and
52 organoids were treated with different regimes. The cocktail for mouse EEC differentiation
53 included: IWP2 (5 μ M; Stemgent), DAPT (10 μ M, Sigma Aldrich) and MEK inhibitor
54 PD0325901 (1 μ M; Sigma Aldrich), while BMP4 (20ng/ml, Peprotech) was added for activation
55 of BMP signaling. In human organoids, differentiation was achieved by withdrawing p38 MAPK
56 inhibitor SB202190, TGFbeta inhibitor A83, Nicotinamide and Wnt conditioned medium from
57 the culture medium as described previously³⁰. Differentiation into EECs was performed by on
58 top treating with DAPT (10 μ M, Sigma Aldrich) and MEK inhibitor PD0325901 (500nM; Sigma
59 Aldrich), BMP4 (20ng/ml, Peprotech) was added for activation of BMP signaling.

60 **Immunostainings**

61 Whole organoids were collected by gently dissolving the BME in ice-cold medium, and
62 subsequently fixed at RT in 4% formalin (Sigma) for at least 6 hours. Next, organoids were
63 permeabilized and blocked in PBS containing 0,5% Triton X-100 (Sigma) and 2% normal
64 donkey serum (Jackson ImunoResearch) for 30 min at room temperature. Organoids were
65 incubated for 2 hr at room temperature in blocking buffer containing primary antibodies. Primary
66 antibodies used were goat anti-Chromogranin A (1:500; Santa Cruz), goat anti-Cholestocystokin
67 (sc-21617,1:100; Santa Cruz), rabbit anti-Neurotensin (sc-20806,1:100; Santa Cruz), goat anti-
68 Secretin (sc-26630,1:100; Santa Cruz), goat anti-Somatostatin (sc-7819, 1:100; Santa Cruz), goat
69 anti-Serotonin (ab66047, 1:1000, Abcam), rabbit anti-Gastric inhibitory polypeptide (ab22624-

70 50, 1:500;Abcam), goat anti-GLP1 (sc-7782, 1:100; Santa Cruz), rabbit anti-GLP1 (ab22625,
71 1:200; Abcam), rabbit anti-Peptide YY (ab22663, 1:500; Abcam) and guinea pig anti-Substance
72 P (1:200, ab10353; Abcam). Organoids were incubated with the corresponding secondary
73 antibodies Alexa488, 568 and 647 conjugated anti-rabbit and anti-goat (1:1000; Molecular
74 Probes) in blocking buffer containing DAPI (1;1000, Invitrogen). Sections were embedded in
75 Vectashield (Vector Labs) and imaged using a Sp8 confocal microscope (Leica). Image analysis
76 was performed using ImageJ software.

77 For immunohistochemistry of organoids within the BME (Figure S4), medium was removed
78 from the wells and replaced with 4% formalin for 1 hour. Next, organoids were washed with
79 PBS, permeabilized and blocked in PBS containing 0,5% Triton X-100 (Sigma) and 2% normal
80 donkey serum (Jackson ImunoResearch) for 30 min at room temperature. The wells were
81 incubated for 2 hr at room temperature in blocking buffer containing primary antibodies. After
82 washing, secondary antibodies were added for 1 hr at room temperature in blocking buffer.
83 Organoids were subsequently imaged within the plate using a Sp8 confocal microscope (Leica).

84 For immunohistochemistry of mouse intestinal tissue, intestines were first flushed with 4%
85 formaldehyde. Next, intestines were fixed for 6 hours at RT in 4% formalin. The tissue was
86 either embedded in paraffin or Tissue-Tek O.C.T. for cryosectioning, and stained as described
87 previously^{6,36}.

88 Quantification of number/location of EECs on intestinal section images were performed in
89 ImageJ software, as well as the intensity of Venus levels in the live cell imaging experiment in
90 Figure S2e-f. Analysis of Glp1⁺ cell numbers and/or position in Figure 1a-c, Figure 4a-c and
91 Figure S5 were performed in the ileum, and all other hormones were counted along the whole SI
92 tract.

93 All quantifications were performed on the raw, unprocessed images.

94 **RNA isolation and quantitative PCR**

95 For qPCR analysis and bulk RNA sequencing, RNA was isolated from organoids using the
96 RNaseasy kit (QIAGEN) as instructed in the manufacturer's protocol. PCR analysis was
97 performed using the SYBR-Green and Bio-Rad systems as described³⁷. PCR reactions were
98 performed in duplicate with a standard curve for every primer. Changes in expression were
99 calculated using CFX manager software (Bio-Rad). Primers were designed using the NCBI
100 primer design tool. Primers used in this study are presented in Supplementary Table 1.

101

102 **Glp1 and Secretin secreted peptide**

103 The supernatant from organoids was collected after 2-hour stimulation with Forskolin. GLP-1
104 concentration in the supernatant was measured with a GLP-1 EIA Kit (Rab0201, Sigma, detects
105 both full length and N-terminal cleaved GLP-1) using the manufacturer's protocol. Secretin
106 concentration was measured with a Secretin EIA kit (EK-067-04, Phoenix Pharmaceuticals)
107 using the manufacturer's protocol.

108

109 **Statistical analysis**

110 Two sided t-tests were performed for all statistical analyses. Precise p-values are mentioned in
111 the corresponding figures, and significance level was set at $p < 0.05$. In each figure legend, the
112 number of biology replicates is mentioned for the corresponding experiment ($n=x$). For figures
113 where representative images are shown, the number the experiment has been repeated is
114 mentioned in the legend.

115 For immunohistochemistry, we counted the following number of cells, of organoids or length of
116 intestine; at least 50 cells per hormone and replicate intestine (Fig. 1b-e, n=4 mice), at least 150
117 tdTomato⁺ cells per co-staining and replicate intestine (Fig. 1f-g, n=4 mice), at least 3 organoids
118 per hormone and replicate (Fig. 2a-b, n=2 biologically independent experiments), 10 organoids
119 per hormone and replicate (Fig. S4a, n=2 biologically independent experiments), 10mm of the
120 proximal small intestine for Tac1 (Fig. 4b-c, n=4 mice per treatment), 30mm of the distal small
121 intestine for Glp1 (Fig. 4b-c, n=4 mice per treatment). mice per genotype) and at least 50 cells
122 per hormone and replicate intestine (Fig. S5b, n=2 mice per genotype),

123

124 **Bulk and single cell RNA sequencing**

125 For bulk RNA sequencing analysis, organoids stimulated with EEC BMPhigh or EEC BMPlow
126 media for 4 days were collected and dissociated in RTL buffer (RNeasy Mini kit, Quiagen).
127 Total RNA was isolated accordingly to manufacturer's instruction (RNeasy Mini kit, Quiagen).
128 Sequencing libraries were prepared based on a modified CELseq2 method¹⁹. Briefly, 1 ng of
129 RNA was reverse transcribed using the Ambion kit and in vitro transcription was performed
130 using 1 ng of cDNA as template. The aRNA was then used to prepare sequencing libraries.
131 Samples were sequenced with sequenced paired-end at 75 bp read-length the on Illumina
132 NextSeq.

133 For single cell RNA sequencing, organoids were first dissociated into single cells through
134 mechanical disruption, after 15 min of Trypsin treatment at 37°C (TrypLE Express; Life
135 Technologies). Next, cells were immediately sorted using a BD FACS Aria (BD Biosciences).
136 For single cell sequencing experiment, cells were sorted as single cells into 384-well plates

137 containing ERCC spike-ins (Agilent), RT primers and dNTP (Promega) as described before.
138 Plates were prepared using Mosquito® HTS (TTPlabtech). Single cell RNA-sequencing libraries
139 were prepared following the SORT-seq protocol¹⁸, which is based on CEL-seq2 method¹⁹.
140 Briefly, cells were first lysed 5 min at 65°C, and RT and second strand mixes were dispensed by
141 the Nanodrop II liquid handling platform (GC biotech). Single cell double stranded cDNAs were
142 pooled together and in vitro transcribed for linear amplification. Illumina sequencing libraries
143 were prepared using the TruSeq small RNA primers (Illumina) and sequenced paired-end at
144 75 bp read length the Illumina NextSeq.

145 **RNA-sequencing data analysis**

146 Paired-end reads from Illumina sequencing were aligned to the mouse transcriptome genome by
147 BWA³⁸. For RNA-seq bulk data, normalization and differential gene expression analyses were
148 performed using the DESeq2 package³⁹ and visualized as volcano plots. For single cell RNA-seq
149 data, read counts were first corrected for UMI barcode by removing duplicate reads that had
150 identical combinations of library, cell-specific, and molecular barcodes and were mapped to the
151 same gene. For each cell barcode the number of UMIs for every transcript was counted, and
152 transcript counts were then adjusted to the expected number of molecules based on counts, 256
153 possible UMI's and poissonian counting statistics⁴⁰. Samples were then normalized by
154 downsampling to a minimum number of 3000 transcripts/cell. Cells with fewer transcripts were
155 excluded from the analyses. RaceID2 was used to cluster cells based on k-medoid method²⁰. All
156 data analyses, quantification and data visualization were run on Rstudio. In total, we sequenced
157 2880 cells and, after applying a filtering criteria of 3000 expressed transcripts/cell, 820 cells
158 were retained for further analysis.

159

160

161 **Data availability**

162 Bulk and single-cell RNA-seq data that support the findings of this study have been deposited in
163 the Gene Expression Omnibus (GEO) under accession code GSE114988.

164

165 Source data for Fig. 1c, 1e, 1g, 2b, 2e, 4a, 5b, 5c, 6b and Supplementary Fig. 1a, 2a, 2b, 2d, 3b,
166 4b, 4c, 5a, 5b and 6 have been provided as Supplementary Table 2. All other data supporting the
167 findings of this study are available from the corresponding author on reasonable request.

168 **References**

169

- 170 36. Farin, H. F. *et al.* Visualization of a short-range Wnt gradient in the intestinal stem-cell
171 niche. *Nature* **530**, 340–343 (2016).
- 172 37. Muñoz, J. *et al.* The Lgr5 intestinal stem cell signature: robust expression of proposed
173 quiescent ‘+4’ cell markers. *EMBO J.* **31**, 3079–3091 (2012).
- 174 38. Li, H. & Durbin, R. Fast and accurate short read alignment with Burrows-Wheeler
175 transform. *Bioinformatics* **25**, 1754–1760 (2009).
- 176 39. Love, M. I., Huber, W. & Anders, S. Moderated estimation of fold change and dispersion
177 for RNA-seq data with DESeq2. *Genome Biol.* **15**, 550 (2014).
- 178 40. Grün, D., Kester, L. & van Oudenaarden, A. Validation of noise models for single-cell
179 transcriptomics. *Nat. Methods* **11**, 637–640 (2014).

180

181

182

183

184

185

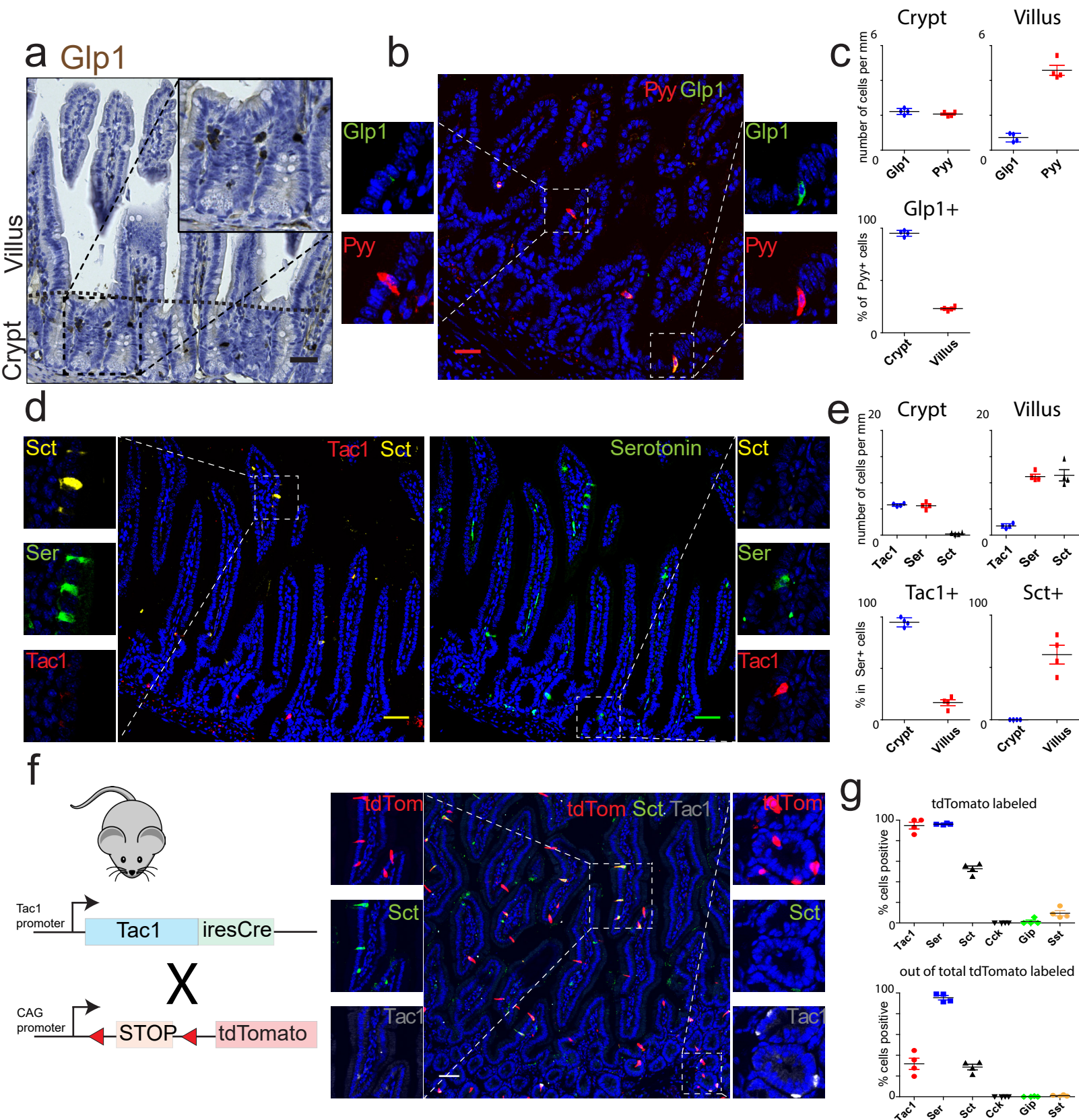


Figure 1 Enteroendocrine cells differentially express hormones along the crypt-villus axis

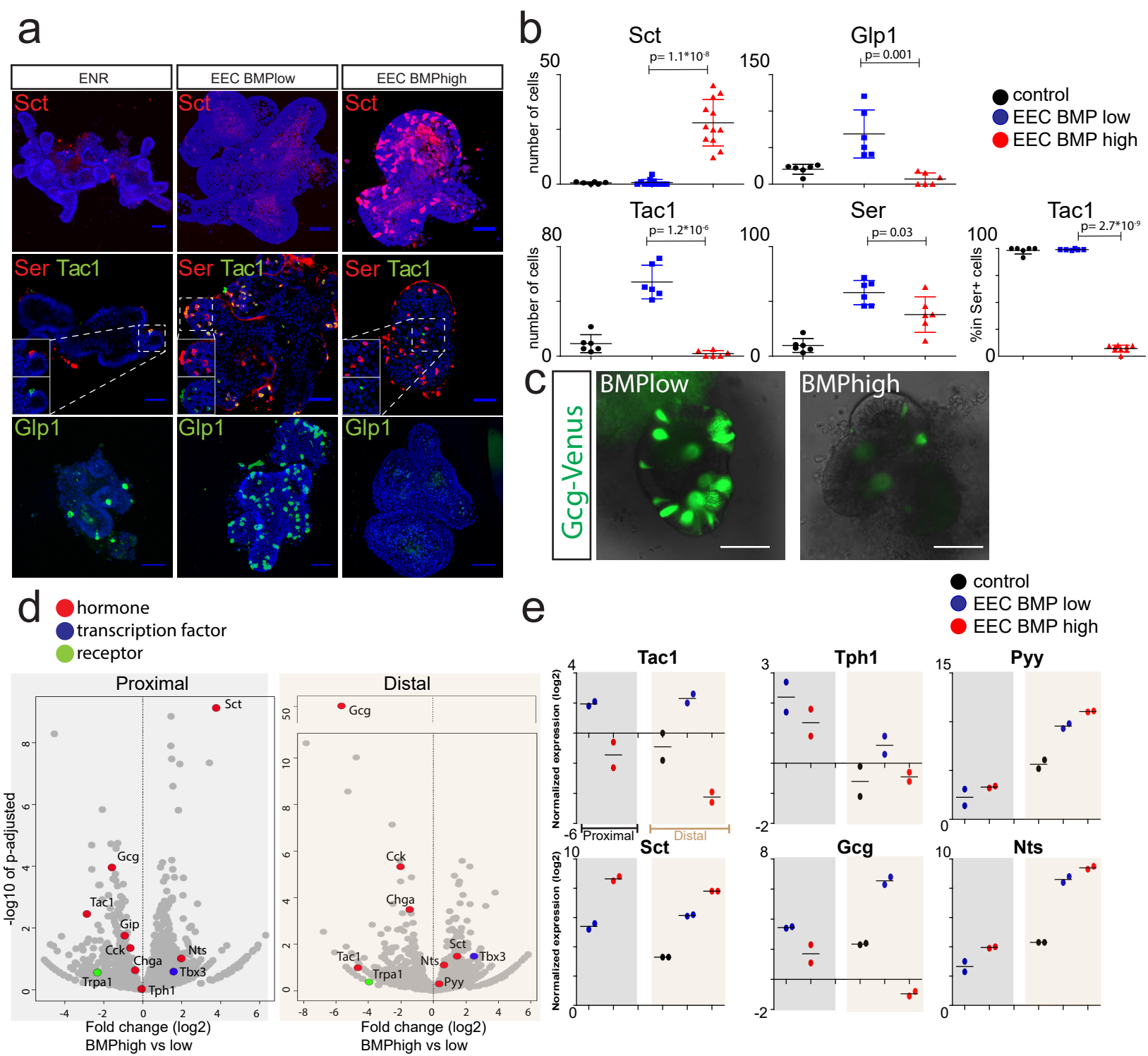


Figure 2 Activation of BMP signaling induces Villus-like hormone signature in mouse EECs.

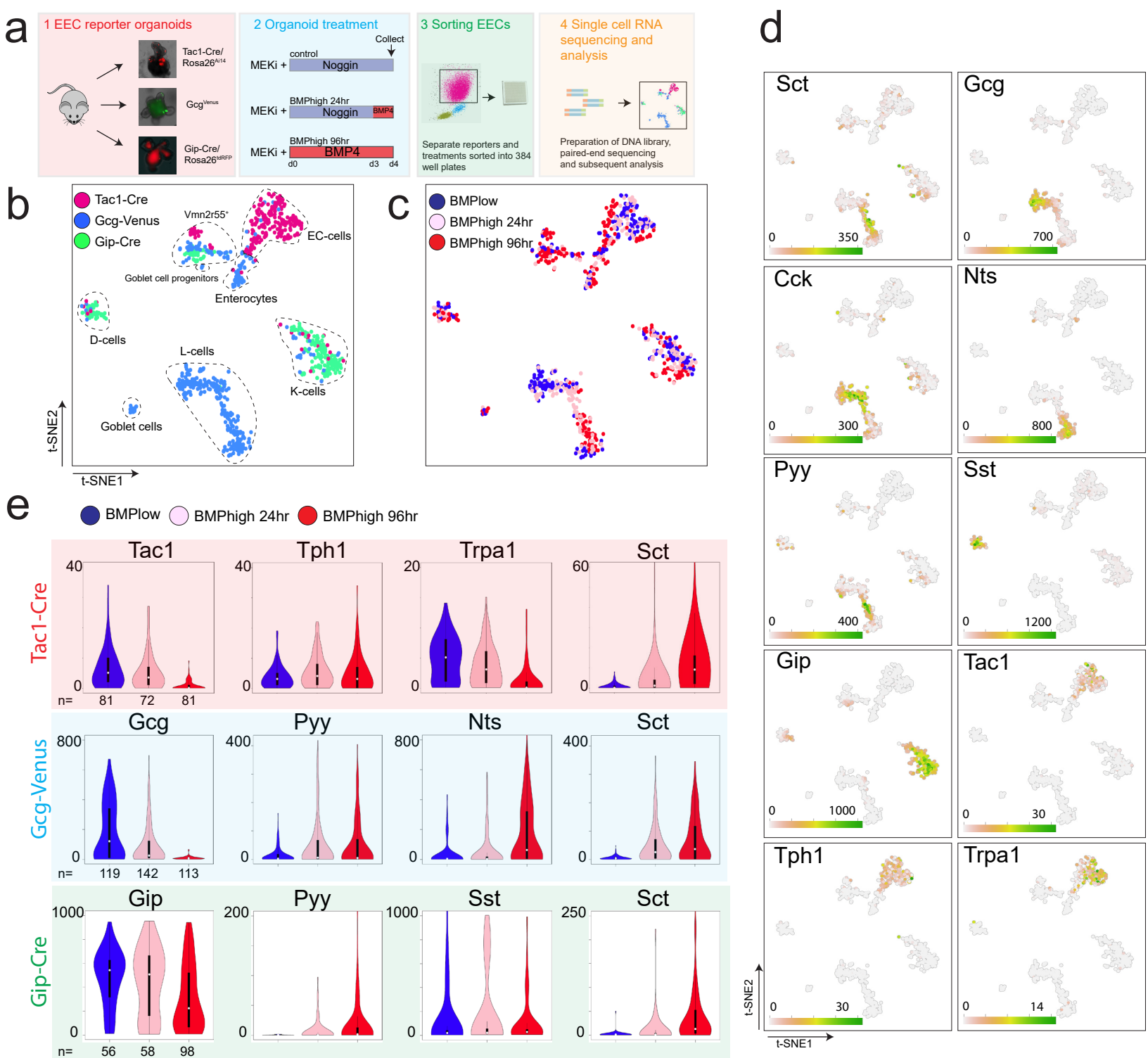


Figure 3 Single cell RNA sequencing reveals BMP regulated plasticity among different EEC subtypes.

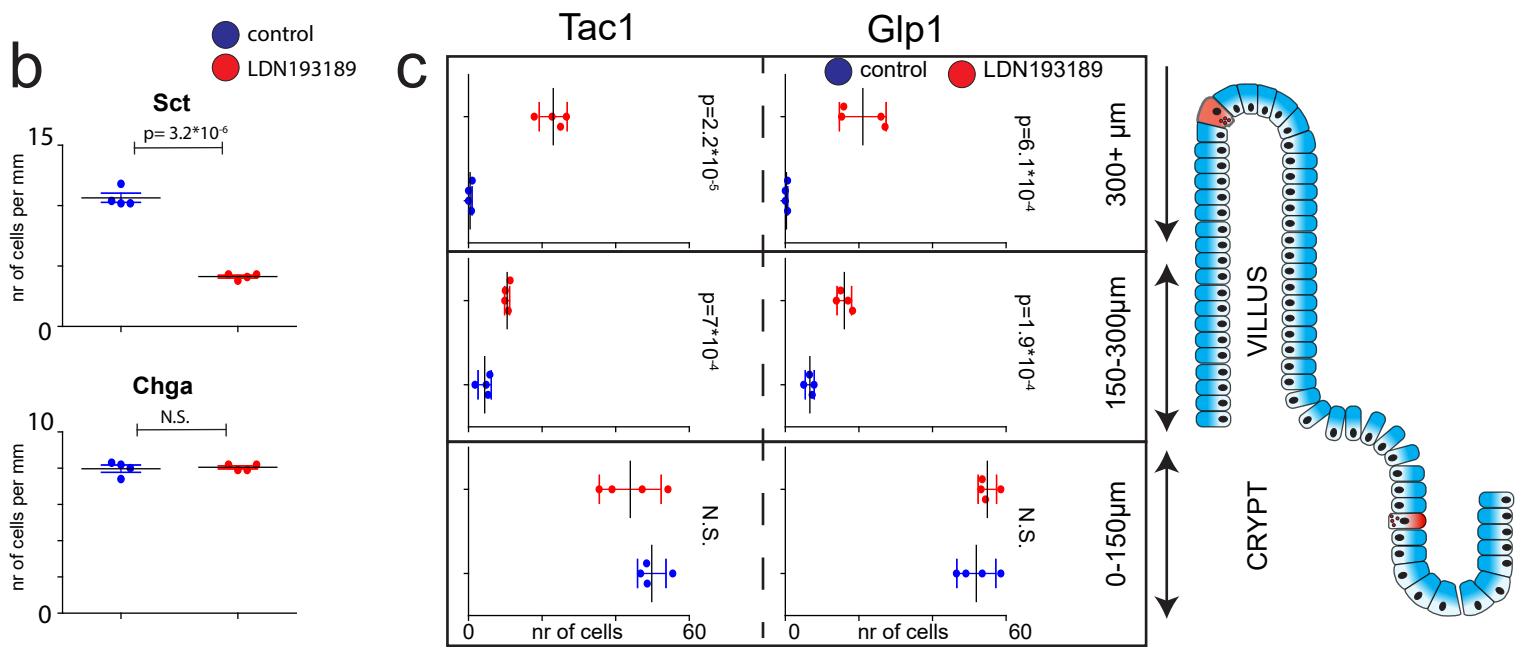
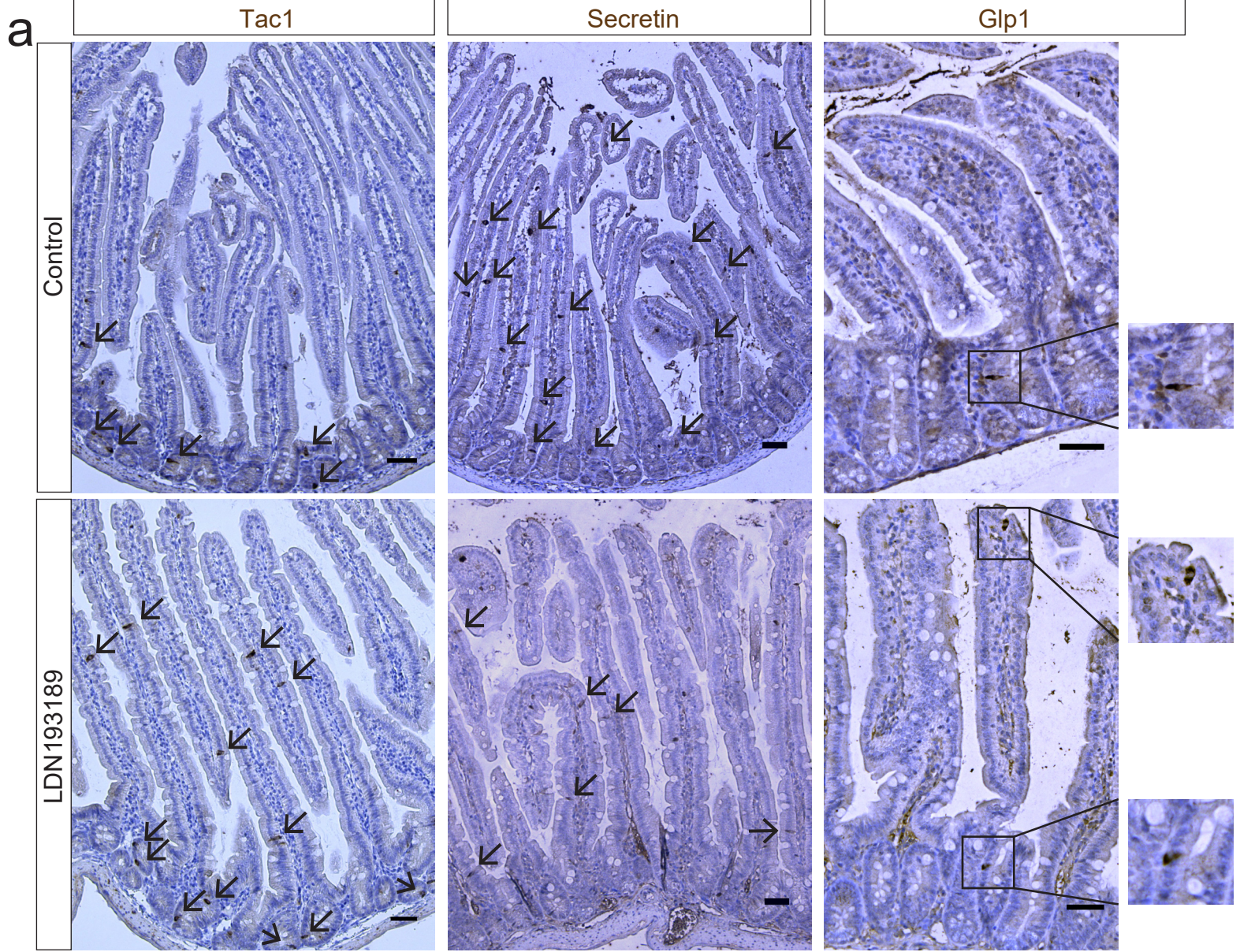


Figure 4 Manipulation of BMP gradient alters hormone expression in mice.

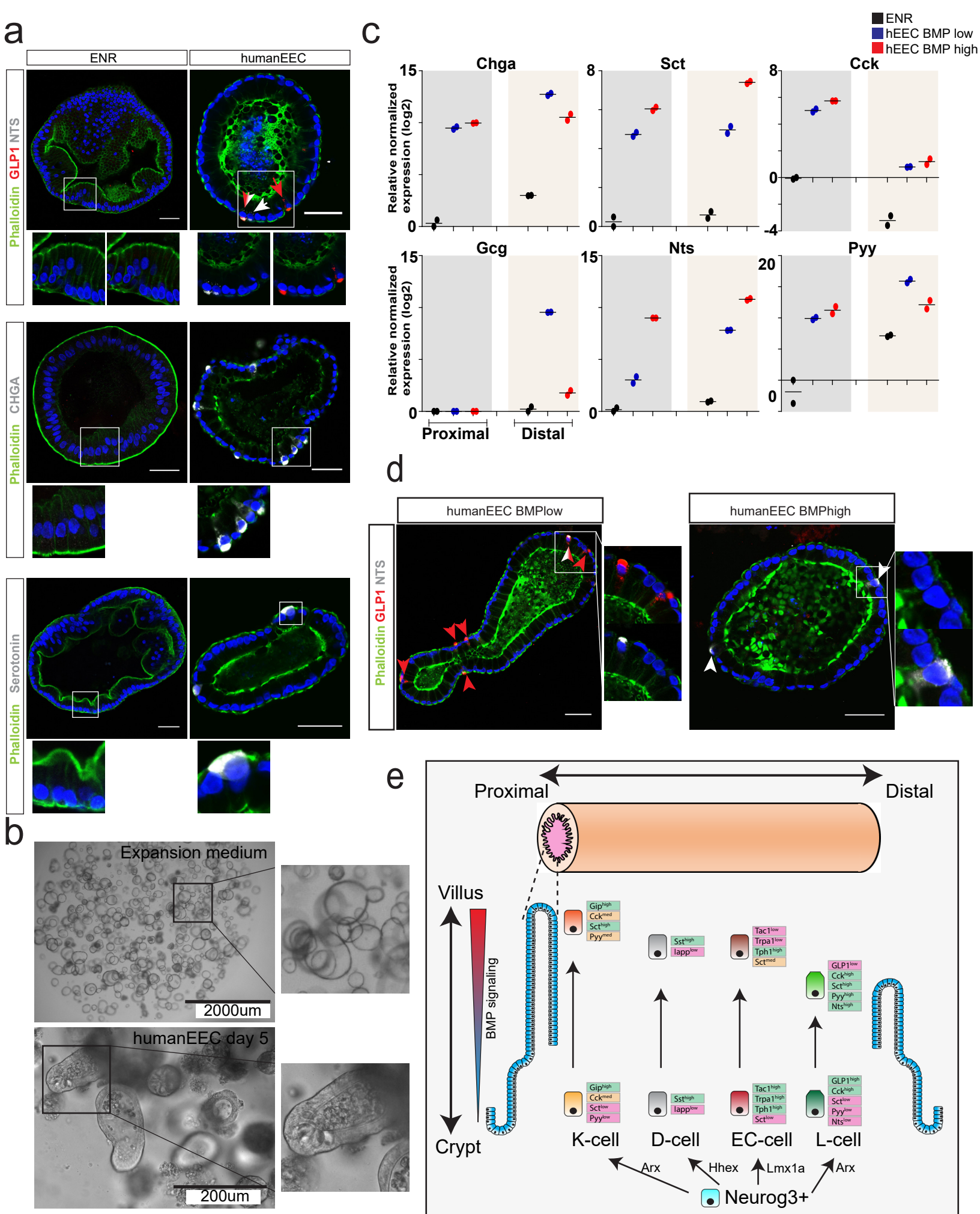


Figure 5 New human EEC differentiation protocol implies conserved BMP-controlled hormone expression